Microporous and Mesoporous Materials 359 (2023) 112648

Contents lists available at ScienceDirect

Microporous and Mesoporous Materials

journal homepage: www.elsevier.com/locate/micromeso

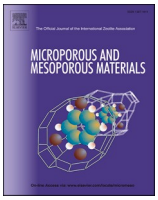

Influence of polymer modification on intra-MOF self-diffusion in MOF-based mixed matrix membranes

Amineh Baniani [a], Matthew P. Rivera [b], João Marreiros [b], Ryan P. Lively [b], Sergey Vasenkov [a,*]

[a] Department of Chemical Engineering, University of Florida, Gainesville, FL, 32611, USA
[b] School of Chemical & Biomolecular Engineering, Georgia Institute of Technology, Atlanta, GA, 30332, USA

ARTICLE INFO

Keywords:
Diffusion
PFG NMR
Mixed-matrix membranes
MOF
Polymer crosslinking

ABSTRACT

Mixed-matrix membranes (MMMs) represent a promising membrane type for gas and liquid separations. Such membranes can be formed by dispersing crystals of metal–organic frameworks (MOFs) in polymers. For liquid separations, crosslinked polymers are desirable because crosslinking reduces polymer dilation and plasticization effects by liquid sorbates. However, polymer crosslinking processes can unfavorably change transport and related structural properties of MOF fillers. In this work, ^{13}C pulsed field gradient (PFG) NMR was used to investigate possible changes in intra-MOF self-diffusion of *p*-xylene and *o*-xylene after MMM polymer crosslinking. The studied MMMs were formed by dispersing MOF crystals of the type ZIF-71 in Torlon (a poly(amide-imide)) or Matrimid (a polyimide) polymers. The reported PFG NMR data indicate that the polymer crosslinking process used does not influence the intra-ZIF diffusivities when all effects on these diffusivities that are related to diffusing molecules crossing over the crystal boundaries or reflected away from these boundaries are removed. In contrast, these data show that the crosslinking process resulted in a significant decrease of the effective size of ZIF-71 crystals inside the studied MMMs, especially in the ZIF-71/Matrimid MMM. This crystal size decrease is attributed to a partial degradation of the ZIF-71 crystals inside the MMMs due to the crosslinking process. This conclusion was found to be in agreement with the results of electron microscopy analysis. PFG NMR studies and data analysis similar to those presented here can be used for quantifying any types of MOF crystal degradation inside MOF-based MMMs.

1. Introduction

Membrane-based separations have emerged as attractive energy-efficient alternatives for gas and liquid separations. Mixed-matrix membranes (MMMs), composed of organic/inorganic permeable fillers dispersed within a polymer phase [1–6], are potentially attractive membrane materials for challenging separation processes. MMMs conceptually combine the superior selectivities of fillers with the functionality and mechanical properties of the pure polymers. MMMs reported in the literature have exhibited enhanced separation properties relative to pure polymeric membranes [7–12]. One promising type of fillers recently implemented in the fabrication of MMMs are zeolitic imidazolate frameworks (ZIFs), a subgroup of metal organic frameworks (MOFs). Exceptional molecular sieving capability of ZIFs arises from their large surface area, high adsorption capacity, tunable ultra-microporous pore apertures, and excellent chemical and thermal stabilities [13–16].

There is a wealth of simulation and experimental studies on ZIF-based MMMs fabricated with different ZIF types including ZIF-8 and ZIF-11 (see, for example, refs [17–26]). Recently, ZIF-71-based MMMs were also investigated for their capability in separations of mixtures of liquid molecules, which have sizes exceeding those of light gases [27–29]. ZIF-71 consists of dichloromidazole ligands and zinc metal centers with nominal pore aperture of 4.2 Å resulting in a RHO topology [14,15,30]. The relatively large aperture of ZIF-71 makes it an ideal candidate for separation of liquid sorbates.

Due to non-uniform structural properties of MMMs and the resulting complexity of the diffusion process, it is desirable to quantify diffusion in different components of MMMs separately. In particular, microscopic diffusion measurements using pulsed field gradient (PFG) NMR can resolve sorbate diffusion inside the polymeric phase and also inside filler particles of MMMs. As already discussed in our previous papers [31–33] as well as in works of others [34–37] for the case of gas separations, transport properties of guests within the MOF component of MMMs can

* Corresponding author.
E-mail address: svasenkov@che.ufl.edu (S. Vasenkov).

https://doi.org/10.1016/j.micromeso.2023.112648
Received 6 March 2023; Received in revised form 10 May 2023; Accepted 14 May 2023
Available online 18 May 2023

change owing to the confinement of MOF particles in the MMMs. A reduced MOF framework flexibility due to confinement of MOF particles in the polymer was identified as the main reason for such transport property change. For the case of liquid separations, a polymer crosslinking in MOF-based MMMs is desirable because it can inhibit polymer dilation and plasticization effects. There is a concern, however, that the crosslinking process can modify the transport and related structural properties of the MOF crystals (i.e., lead to crystal surface changes and/or defect formation). The current work focuses on investigating possible changes in intra-MOF diffusion in MMMs induced by polymer crosslinking and on the potential for PFG NMR to quantify such changes. To this end, ^{13}C PFG NMR was used to measure single component *p*-xylene and *o*-xylene diffusion in ZIF-71 MMMs in which the polymer matrix is crosslinked. The intra-ZIF diffusion data obtained for these MMMs were compared with those measured for the corresponding beds of ZIF crystals used to prepare the MMMs. It is important to note that we have already reported previously the PFG NMR measurements of intra-ZIF self-diffusivities of the xylene isomers in ZIF-71-based MMMs without any crosslinking [38,39].

2. Experimental

2.1. Preparation of ZIF-71

ZIF-71 was prepared following a previously reported procedure [39]. Briefly, 0.585 g of zinc acetate dehydrate (2.67 mmol) was dissolved in 100 mL of anhydrous methanol. Separately, 1.461 g of 4,5-dichloroimidazole (10.67 mmol) was dissolved in 100 mL of anhydrous methanol. Next, 0.581 g of imidazole (8.53 mmol, 0.8 equivalents relative to 4, 5-dichloroimidazole) was added to the 4,5-dichloroimidazole solution and dissolved with sonication. The two solutions were combined and allowed to sit undisturbed at room temperature for two days. The product was isolated by centrifugation. This product was washed with N-methyl-2-pyrrolidone (NMP) for three days, replacing with fresh NMP each day by decanting without centrifugation. The large ZIF crystals were then washed with methanol for three days, replacing with fresh methanol each day, and dried at 383 K under vacuum overnight. Figs. S1 and S2 show the particle size distribution and SEM images of the sample, respectively. The crystal size distribution was obtained by analyzing SEM images in the image processing software ImageJ and measuring the size of ~100 randomly selected crystals. The powder x-ray diffraction patterns are presented in Fig. S3. Despite a minor shift to the right, the patterns show good consistency with the simulated structures (Fig. S3).

2.2. MMM preparation and polymer crosslinking

2.2.1. Crosslinked Torlon MMM film preparation

Torlon film preparation was adapted from a previous work [39]. 0.7 g of ZIF-71 and 0.3 g of dried Torlon were dissolved in 5.6 g NMP. The mixture was placed on a rolling mixer under a heat lamp (creating an ambient temperature of ~328 K) until complete polymer dissolution, usually 1–2 days. The mixture was sonicated 10 times in 30 s intervals with a Branson Digital Sonifier set at 30% amplitude, with approximately 1 min between sonications. A clean glass plate was heated on a hot plate set to 393 K in a fume hood. The dope was cast on the glass plate using a 10 mil casting knife. The resulting film was allowed to dry on the plate overnight. The film was then washed with methanol for one day. To carry out the crosslinking, the film was submerged in a solution of 5 w/v% (i.e., 5 g/100 mL of solution) p-xylylenediamine in anhydrous methanol for two days. The crosslinked film was washed with methanol for three days, replacing with fresh methanol each day. After washing, the film was dried at 383 K under vacuum overnight. Figs. S4A and S5A show the SEM images of Torlon film and the resulting ZIF-71/Torlon MMM, respectively. The crystal size distribution in the MMM was obtained by analyzing SEM images in the image processing software ImageJ and measuring the size of ~100 randomly selected crystals. The effectiveness of the crosslinking reaction was probed by Transmission FTIR spectroscopy. FTIR spectra were collected under quantitative conditions with fixed gain for accurate sample comparison (Fig. S6). FTIR characterization was limited to ZIF-free film samples to facilitate quality spectra and ease of interpretation. Spectra analysis revealed the peak suppressions at 1380 cm^{-1}, assigned to imide C–N–C stretching, and 1720 and 1790 cm^{-1}, assigned to asymmetric imide C═O stretching. Signal suppression is also observed in the range 2700–3200 cm^{-1}, likely a result of trace solvent (MeOH, O–H stretch) present in the unmodified Torlon sample and absent in the treated film. Furthermore, a decline in C–H stretch bands from the polymer's aromatic backbone (sp^2 carbon C–H stretch), due to changes in charge density, also contributes to the signal suppression in question thus supporting the occurrence of successful crosslinking. In sum, the spectral changes in the crosslinked film substantiate the notion of imide bond breaking in line with the expected film modification after p-xylylenediamine treatment, as depicted in Fig. 1A.

2.2.2. Crosslinked Matrimid MMM film preparation

To create the crosslinked Matrimid MMMs, 0.7 g of ZIF-71 and 0.3 g of dried Matrimid were dissolved in 5.6 g chloroform. The mixture was placed on a rolling mixer until complete polymer dissolution, which occurred within one day, typically. The mixture was sonicated 10 times in 30 s intervals with a Branson Digital Sonifier set at 30% amplitude, with approximately 1 min between sonications. A glovebag with a clean glass casting plate was evacuated with nitrogen and then sealed and saturated with chloroform vapors overnight. The membrane dope was quickly placed into the glovebag, which was then resealed. The dope was cast on the glass plate using a 10 mil casting knife. The resulting film was allowed to dry on the plate overnight. The rest of the preparation was identical to the Torlon film. Figs. S4B and S5B present the SEM images of Matrimid film and the ZIF-71/Matrimid MMM, respectively. The crystal size distribution in the MMM was obtained by analyzing SEM images in the image processing software ImageJ and measuring the size of ~100 randomly selected crystals. The crosslinking reactions of Torlon and Matrimid are given in Fig. 1A and B, respectively.

2.3. NMR sample preparation

All NMR samples were prepared following an identical procedure described in Refs. [38,39]. Briefly, the vertically oriented strips of ZIF-71-based MMMs with a height of about 30 ± 5 mm were tightly packed inside a thin-wall 5 mm NMR tube (Wilmad-LabGlass). The corresponding ZIF-71 crystals were also placed into the same NMR tubes to achieve tightly packed beds with a height of 20 ± 5 mm. A custom-made vacuum system was used to remove all sorbates from the NMR samples under high vacuum overnight at 373 K before introducing the desired sorbates. After degassing, a desired amount of a liquid sorbate was introduced into the NMR tube by sorbate condensation using liquid nitrogen. The samples were flame sealed and removed from the vacuum system upon loading. The following sorbates were used in this study: 99% isotopic purity $^{13}C_2$-labeled *p*-xylene (Sigma-Aldrich) or 99% isotopic purity $^{13}C_2$-labeled *o*-xylene (Sigma-Aldrich).

The sorbate amount in the samples were determined following the procedure discussed in Refs. [38,39]. To obtain the liquid sorbate loading in a studied sample, the measured intensity of the ^{13}C NMR signal of this sorbate (i.e. area under the ^{13}C NMR spectrum) was used. To relate the ^{13}C NMR signal intensity to the number of molecules in the studied samples, a reference sample with a known amount of bulk liquid sorbate (no membrane or ZIF added) was measured by ^{13}C NMR. Under our experimental conditions, it was possible to obtain the intra-ZIF sorbate loadings in the MMMs using the total sorbate signal in the MMM samples and the signal fractions from the ZIF phase of the MMM. These fractions were obtained from the T_2 NMR relaxation measurements (see section 2.4), which reveal only two ^{13}C T_2 NMR relaxation times and the related signal fractions. These fractions were assigned to

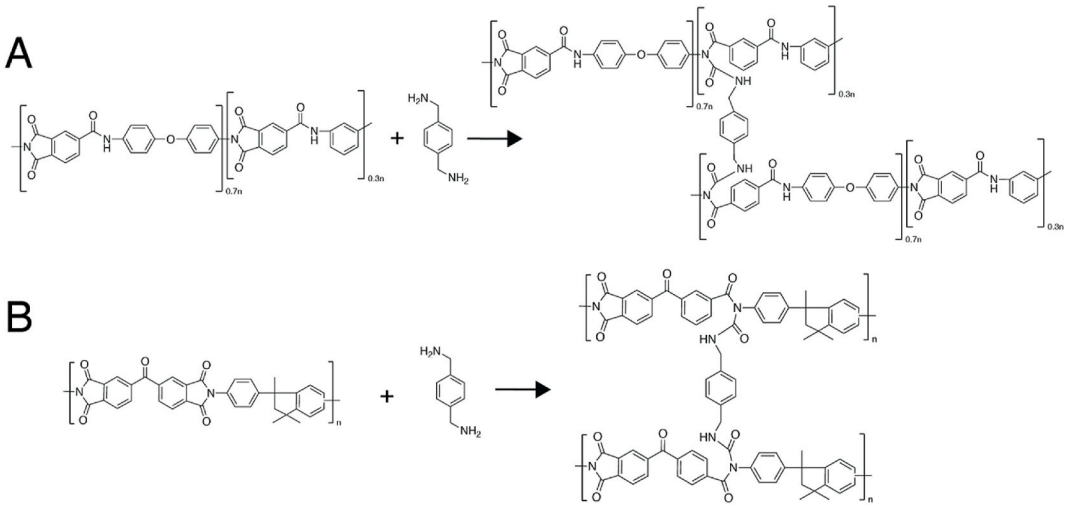

Fig. 1. Crosslinking reaction of p-xylylenediamine with Torlon (A) and Matrimid (B).

sorbate molecules inside and outside of ZIF-71 crystals in MMMs. No measurable bulk liquid fraction was observed. The latter observation is consistent with the results of ^{13}C PFG NMR measurements reported below. Using ^{13}C T_2 NMR relaxation measurements in a similar way, we have also determined the intra-ZIF component fractions and the corresponding intra-ZIF sorbate concentrations for ZIF-71 bed samples. The estimated intra-ZIF concentrations at 273 K are presented in Table 1. It can be seen that, within uncertainty, all intra-ZIF concentrations were the same under our experimental conditions.

2.4. NMR measurements

A wide bore 14 T Avance III HD spectrometer (Bruker Biospin) operating at a^{13}C resonance frequency of 149.8 MHz was used to perform all ^{13}C NMR measurements. ^{13}C PFG NMR instead of more common ^{1}H PFG NMR was used to take advantage of the larger T_2 NMR relaxation times of ^{13}C nuclei than ^{1}H nuclei in the studied samples. For *p*-xylene and *o*-xylene, the ^{13}C PFG NMR spectrum exhibited a single line with the chemical shift of around 21 and 20 ppm, respectively. In order to determine the ^{13}C PFG NMR chemical shift, an NMR reference standard of 40% 1,4-dioxane in benzene-d_6 (Sigma-Aldrich) was used.

Sine-shaped magnetic field gradients with strengths up to 18 T/m were generated using a *diff30* diffusion probe (Bruker Biospin) at 14 T. Duration of magnetic field gradients were between 1 and 2 ms. The total time of a single ^{13}C PFG NMR diffusion experiment varied between 3 and 6 h with the total number of scans between 64 and 128. The repetition delays were chosen between 7 and 13 s to be at least 1.5 times greater than the respective T_1 NMR relaxation times. To ensure sorption equilibrium, all NMR samples were kept inside the magnet at 273 K for a minimum of 1 h before conducting any NMR measurements. During the measurement time interval, selected NMR experiments were repeated after waiting times of several hours to verify that there are no changes in the experimental results as a function of the waiting time. The observed consistency of the experimental results measured after several hours indicated no changes in the intra-ZIF sorbate loadings.

Table 1
Intra-ZIF and intra-polymer sorbate loading of the studied sorbates in ZIF-71 crystal beds and ZIF-71-based MMM samples obtained by^{13}C NMR at 273 K.

Sample	Intra-ZIF Sorbate Loading (mmol/g)[a]	Intra-polymer Sorbate Loading (mmol/g)[a]
ZIF-71 loaded with *p*-xylene	1.3	–
ZIF-71 loaded with *o*-xylene	1.2	–
ZIF-71/Torlon MMM loaded with *p*-xylene	0.9	0.6
ZIF-71/Torlon MMM loaded with *o*-xylene	0.8	0.7
ZIF-71/Matrimid MMM loaded with *p*-xylene	0.8	0.8
ZIF-71/Matrimid MMM loaded with *o*-xylene	0.8	0.9

[a] 30% experimental uncertainty.

To conduct the diffusion measurements, the 13-interval PFG NMR pulse sequence with an addition of the eddy current delay was utilized [40,41]. PFG NMR attenuation curves, which are dependencies of the normalized PFG NMR signal intensities ($\Psi = \frac{S(g)}{S(g\approx 0)}$), viz. signal attenuation, on the magnetic field gradient amplitude (g), were used to acquire self-diffusion coefficients (D) [40,42–46]:

$$\Psi = \frac{S(g)}{S(g \approx 0)} = \exp\left(-\frac{< r^2(t) > q^2}{6}\right) = \exp\left(-Dtq^2\right) \quad (1)$$

$< r^2 >$ is the mean square displacement (MSD), $q = \gamma g \delta$, where γ is the gyromagnetic ratio, δ is the effective duration of the magnetic field gradient, and t is the diffusion time described in refs ([40,46,47]). For three-dimensional diffusion, Einstein relation was used to relate MSD to D and t as [42]

$$< r^2(t) >= 6Dt. \quad (2)$$

For two molecular ensembles of the same type of molecules diffusing with different self-diffusivities, Eq. (1), can be re-written as [42–44].

$$\Psi = \frac{S(g)}{S(g \approx 0)} = \sum_{i=1}^{2} p_i \exp\left(-D_i q^2 t\right) \quad (3)$$

where p_i and D_i are, respectively, the signal fraction and self-diffusivity of ensemble i. The experimental errors reported for self-diffusivities were determined based on the reproducibility of the diffusion data measured with several different PFG NMR samples prepared identically.

Longitudinal (T_1) and transverse (T_2) NMR relaxation times of liquid sorbates were determined as discussed in Refs. [38,39] using standard inversion recovery and standard Carr-Purcell-Meiboom-Gill (CPMG) pulse sequences, respectively. In CPMG pulse sequence, tau was set to be 100 μs. The inversion recovery measurements indicated an existence of a single T_1 NMR relaxation time for each sorbate type inside each studied NMR sample (Table S1). The CPMG measurements showed the presence of two molecular ensembles with different T_2 NMR relaxation times, and a bi-exponential fit was used to acquire the T_2 NMR relaxation time values and the corresponding fractions of molecular ensembles. For the ZIF-71 samples, the two molecular ensembles were assigned to the bulk liquid inside the sample (ensemble 1) and molecules located inside

ZIF-71 crystals (ensemble 2). For the MMM samples, the two molecular ensembles were assigned to the liquid sorbate molecules located inside the polymer phase of the MMMs modified by the crosslinking procedure (ensemble 1) and molecules located inside ZIF -71 crystals (ensemble 2). The observation of the T_2 ensemble corresponding to sorbate molecules located inside of the modified polymer phase of the MMMs was initially unexpected in view of our previous data obtained for gases and liquids in similar types of ZIF-based MMMs prepared with the same polymers but without any polymer modifications [31–33,38,39]. This observation will be discussed more in the next section. All NMR relaxation data are presented in Table S1. All reported NMR measurements were performed at 273 K. This temperature was selected because it allowed performing intra-ZIF PFG NMR diffusion measurements for root MSDs sufficiently smaller than the ZIF-71 crystal sizes.

3. Results and discussion

Figs. 2 and 3, and S7 present examples of the measured ^{13}C PFG NMR attenuation curves at 273 K for self-diffusion of *p*-xylene or *o*-xylene in the samples of ZIF-71 MMMs and the corresponding ZIF-71 crystal beds. The PFG NMR attenuation curves obtained for all samples show large deviations from the monoexponential behavior (Eq. (1)), which corresponds to linear dependencies in the semi-logarithmic presentation of Figs. 2 and 3, and S7. Instead of linear dependencies, the attenuation curves exhibit a faster decay at smaller values of q^2t and a much slower decay at larger values of q^2t. In complete analogy with the diffusion data processing performed in our previous studies [38,39], an existence of two molecular ensembles diffusing with different self-diffusivities was assumed. Hence, Eq. (3) was used to describe the measured attenuation curves. The results of least square fitting using Eq. (3) are presented in Figs. 2 and 3, and S7 with the best-fit values of diffusivities and signal fractions are shown in Table 2. The larger diffusivity ensemble (ensemble 1) was assigned to the ensemble of xylene molecules diffusing outside of ZIF-71 crystals. It corresponds to the diffusion in the bulk liquid phase in the ZIF-71 bed samples or inside of the modified polymer phase of ZIF-71-based MMMs, i.e. intra-polymer ensemble in the MMM samples. The smaller diffusivity ensemble (ensemble 2) was assigned to xylene molecules diffusing inside ZIF-71 crystals, i.e. intra-ZIF ensemble. It is important to note that for the slower-diffusing o-xylene the intra-ZIF diffusivities could not be measured inside the MMMs at the smallest diffusion time used in this work (9 ms) because of the signal-to-noise limitations. Such limitations are more significant for MMMs than for ZIF-71 crystal beds because of smaller total number of ZIF-71 crystals in the MMM than in bed samples.

The observation of ^{13}C PFG NMR signal corresponding to the intra-polymer self-diffusion was explained by relatively long ^{13}C T_2 NMR relaxation times of xylene molecules in the modified phase of polymers in MMMs (Table S1). At the same time, no ^{13}C PFG NMR signal corresponding to the intra-polymer self-diffusion of the xylene isomers was observed in pure crosslinked Torlon and Matrimid polymer samples (no ZIF-71 crystals present). As mentioned above, we were unable to detect a^{13}C PFG NMR signal corresponding to the intra-polymer self-diffusion of the xylene isomers in the ZIF-based MMMs prepared with the same polymers, which were not modified [31–33,38,39]. All these data combined with the observation of the relatively fast self-diffusion (Table 2) in the modified polymer phase of the MMMs studied in this work suggest that the crosslinking procedure of the polymer phase of the MMM was influenced by the presence of ZIF-71. As a result of this influence, a polymer phase with either a higher free volume or a defective structure (or a combination of the two) was formed.

It can be seen in Figs. 2 and 3, and S7 that the fraction of intra-ZIF self-diffusion ensemble (ensemble 2) decreases with an increase in the diffusion time (Table 2). It is important to note that the time interval of the PFG NMR sequence during which the T_2 NMR relaxation takes place was held constant when the diffusion time was changed. Hence, the observed changes are not related to NMR relaxation effects. As already discussed in our previous work, such a decrease can likely be attributed to the xylene molecules diffusing away from the ZIF-71 crystals as these molecules encounter the crystal boundaries [38]. Moreover, Table 2 highlights that the fraction of ensemble 1 increases as diffusion time increases. This observation is in agreement with the expectation that as diffusion time increases more xylene molecules will leave ZIF-71 crystals and start diffusing in the polymer phase.

Under our measurement conditions, the values of the root MSD of the intra-ZIF ensemble were observed to be smaller than and/or comparable with the average crystal size in all the studied samples (Fig. 4A and Table 2). It can be seen in Fig. 4A that there is a trend of decreasing intra-ZIF self-diffusivities with increasing root MSDs. In complete analogy with our previously reported measurements [38,39], the observed dependencies of the intra-ZIF self-diffusivity on root MSD were attributed to the influence of the external crystal surface on the diffusion process. For ZIF-71/Matrimid MMM samples, the dependencies of the intra-ZIF self-diffusivity on root MSD were observed to be somewhat stronger, on average, than those for the ZIF-71/Torlon MMM and ZIF-71 crystal bed samples (Fig. 4A). Such stronger dependencies can be due to smaller crystal sizes in the former samples in comparison to the latter samples. Qualitative analysis of the SEM images of both MMM types revealed signs of the external crystal boundary degradation (Figs. S4B and S5B). The crystal degradation is likely a result of the diamine crosslinker disrupting metal-ligand coordination bonds within the crystal structure,

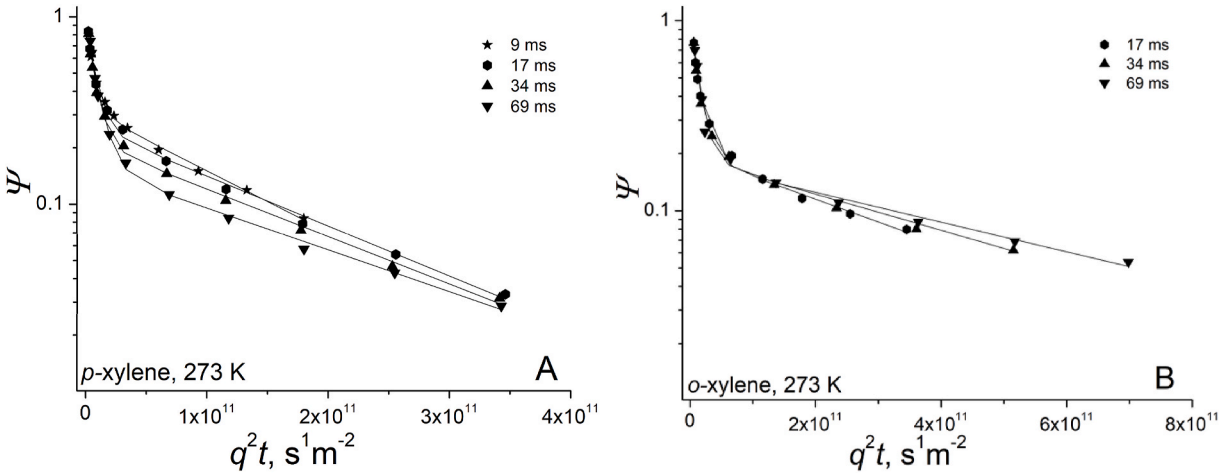

Fig. 2. Examples of ^{13}C PFG-NMR attenuation curves measured for *p*-xylene (A) and *o*-xylene (B) diffusion in a crosslinked ZIF-71/Torlon MMM performed at 273 K and 14 T using the 13-interval pulse sequence. The solid lines represent the results of least-square fitting using Eq. (3).

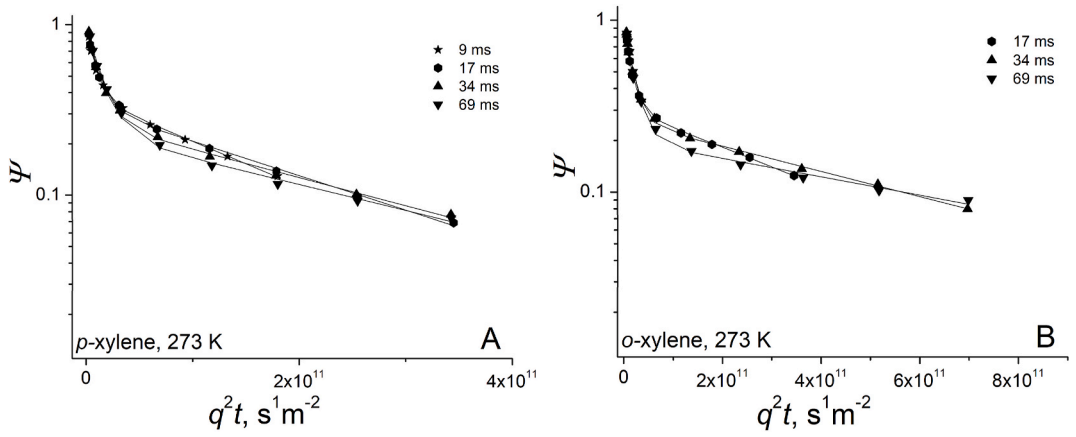

Fig. 3. Examples of ^{13}C PFG-NMR attenuation curves measured for *p*-xylene (A) and *o*-xylene (B) diffusion in a crosslinked ZIF-71/Matrimid MMM performed at 273 K and 14 T using the 13-interval pulse sequence. The solid lines represent the results of least-square fitting using Eq. (3).

Table 2
Diffusion data obtained from the measured^{13}C PFG NMR attenuation curves. Root MSDs were calculated using Eq. (2).

Sample	Sorbate	Diffusion time (ms)	D_1(m^2/s) × 10^{-10}	$<r^2>_1^{1/2} \times 10^{-6}$ (m)	D_2(m^2/s) × 10^{-10}	$<r^2>_2^{1/2} \times 10^{-6}$ (m)	p_1	p_2
ZIF-71 crystal beds	*p*-Xylene	9	6.0 ± 1.2	5.6 ± 0.6	0.075 ± 0.019	0.63 ± 0.08	0.48	0.52
		17	4.5 ± 0.9	6.7 ± 0.7	0.070 ± 0.017	0.8 ± 0.1	0.52	0.48
		34	4.0 ± 0.8	9.0 ± 0.9	0.065 ± 0.016	1.1 ± 0.1	0.58	0.42
		69	4.6 ± 0.9	13.7 ± 1.4	0.056 ± 0.014	1.5 ± 0.2	0.67	0.33
	O-xylene	9	4.2 ± 0.9	4.7 ± 0.5	0.027 ± 0.007	0.37 ± 0.05	0.26	0.74
		17	3.5 ± 0.7	6.0 ± 0.6	0.024 ± 0.006	0.49 ± 0.06	0.28	0.72
		34	3.7 ± 0.7	8.6 ± 0.9	0.022 ± 0.005	0.66 ± 0.08	0.30	0.70
		69	4.8 ± 1.0	14.0 ± 1.4	0.019 ± 0.005	0.9 ± 0.1	0.37	0.63
ZIF-71/Torlon MMM	*P*-xylene	9	1.6 ± 0.4	2.9 ± 0.3	0.076 ± 0.019	0.63 ± 0.08	0.68	0.32
		17	1.3 ± 0.4	3.7 ± 0.4	0.062 ± 0.015	0.8 ± 0.1	0.74	0.26
		34	1.4 ± 0.3	5.3 ± 0.5	0.058 ± 0.015	1.1 ± 0.1	0.78	0.22
		69	1.1 ± 0.3	6.9 ± 0.7	0.051 ± 0.013	1.5 ± 0.2	0.84	0.16
	O-xylene	17	0.7 ± 0.3	2.7 ± 0.3	0.028 ± 0.007	0.53 ± 0.07	0.79	0.21
		34	0.7 ± 0.2	3.9 ± 0.4	0.022 ± 0.006	0.67 ± 0.09	0.80	0.20
		69	0.7 ± 0.2	5.2 ± 0.5	0.018 ± 0.005	0.9 ± 0.1	0.81	0.19
ZIF-71/Matrimid MMM	*P*-xylene	9	1.2 ± 0.3	2.5 ± 0.3	0.061 ± 0.015	0.56 ± 0.07	0.62	0.38
		17	1.0 ± 0.2	3.2 ± 0.3	0.047 ± 0.012	0.68 ± 0.08	0.67	0.33
		34	0.8 ± 0.2	4.1 ± 0.4	0.038 ± 0.010	0.9 ± 0.1	0.73	0.27
		69	0.7 ± 0.1	5.4 ± 0.5	0.035 ± 0.009	1.2 ± 0.2	0.77	0.23
	O-xylene	17	0.7 ± 0.2	2.7 ± 0.3	0.026 ± 0.007	0.51 ± 0.06	0.69	0.31
		34	0.6 ± 0.1	3.4 ± 0.3	0.017 ± 0.004	0.59 ± 0.07	0.74	0.26
		69	0.5 ± 0.1	4.5 ± 0.5	0.012 ± 0.003	0.71 ± 0.09	0.80	0.20

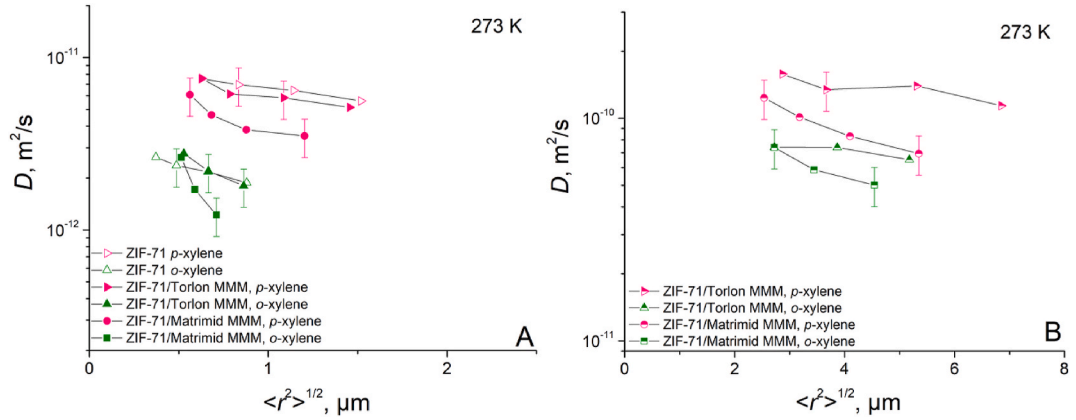

Fig. 4. Intra-ZIF (A) and intra-polymer (B) self-diffusivities of *p*-xylene and *o*-xylene plotted as a function of root MSD for ZIF-71 crystal beds (A, hollow symbols) and ZIF-71 based MMMs (A, filled symbols and/or B, half-filled symbols) at 273 K. The data were measured by the 13-interval PFG NMR sequence at 14 T.

despite the fact that 4,5-dichloroimidazole (pKa 11.01) [48] is a stronger Lewis base than p-xylylenediamine (pKa 9.46) [49]. The high diamine concentrations required to fully crosslink the polymers likely shifted the equilibrium to favor partial substitution into the ZIF framework, which would disrupt or damage the crystal surface. In agreement with this qualitative observation, the average crystal size in the ZIF-71/Torlon MMMs and ZIF-71/Matrimid MMMs was estimated to be ~3.4 μm and ~2.2 μm, respectively, which is smaller than that (~4.1 μm) of the ZIF-71 crystal beds (Fig. 5 and S1). We note that no crystal degradation was observed in previous investigations into uncrosslinked ZIF-71/polyimide MMMs [38,39]. Microporosity of the ZIF crystals embedded within the membrane was confirmed with N_2 physisorption, seen in Fig. S8. Neat ZIF crystals were exposed to the same diamine conditions used during the film crosslinking procedure and characterized by nitrogen physisorption. Calculated BET surface areas were used to probe for potential changes to the ZIF particles' textural features. Surface areas of 943 m^2/g and 919 m^2/g, were determined for the parent and diamine treated films, respectively, suggesting that while some degradation of the crystal surface may occur, the overall ZIF structure retains its structural integrity and microporosity.

In contrast to the intra-ZIF ensemble, under our experimental conditions the values of root MSDs of the intra-polymer ensemble were larger than the average ZIF-71 crystal size in all the studied MMM samples (Table 2). It can be seen in Fig. 3B that the self-diffusivities of this ensemble show a slight decrease as root MSD increases. This behavior can be attributed to a structural inhomogeneity in the polymer phase related to the presence of defects. Indeed, our analysis of the SEM images of the MMMs (Figs. S4B and S5B) indicates formation of defects and/or pockets of free volume with sizes up to several hundreds of nanometers, which can be attributed to the degradation of a fraction of ZIF-71 crystal volume next to the external crystal surface.

In complete analogy with the MMM data processing in our recent publications [38,39], dependencies of the intra-ZIF self-diffusivities on the square root of the diffusion time can be utilized to estimate intra-ZIF self-diffusivities that are not influenced by any effects at the external surface of crystals (D_0). For this purpose, we used an analytical equation proposed by Mitra et al., to quantify external surface effects on self-diffusion inside spheres with radius R

$$\frac{D(t)}{D_0} \approx 1 - \frac{f}{3R}\left(\frac{D_0 t}{\pi}\right)^{0.5}, \quad (4)$$

where $D(t)$ is the diffusion time dependent self-diffusivity for diffusion inside the spheres, D_0 is the corresponding self-diffusivity for diffusion inside the spheres which is not influenced by any effects at the sphere external surface, $f = 4$ for reflecting external surface and $f = 2$ for adsorbing external surface, viz. the case of no transport resistances to cross over the sphere surface [50,51]. In the case of considered ZIF-71 crystals, reflections of molecules from the external crystal surface can occur owing to pore blockage at this surface and/or lower potential energy inside of the crystal compared to the crystal surroundings. In contrast, in crystals with adsorbing external surface, sorbate molecules can exit the crystals without encountering any additional transport resistances at the external surface. The dependencies of the measured intra-ZIF diffusivities on $t^{0.5}$ for all studied samples are presented in Fig. 6. The solid and dotted lines in Fig. 6 correspond, respectively, to the least square fittings of the data for ZIF-71-based MMMs and ZIF-71 crystal beds using Eq. (4). In Fig. 6, the intercept of the best fit lines with the vertical axis yields the values of D_0. These values are shown in Table 3 for each studied sample. Comparison of the data in Table 3 shows that for the same sorbate the values of D_0 are the same, within uncertainty, for all studied MMM and crystal bed samples. Also, there is a good agreement between the D_0 values in Table 3 and the corresponding data for the MMMs without polymer modification [38,39]. These data present the quantitative proof that despite the ZIF-71 crystal degradation in the MMMs, the ZIF-71 transport properties away from the crystal boundaries remain unchanged. This type of analysis has not been demonstrated for MMMs before. Clearly, it can be beneficial for quantifying any type of MOF crystal degradation inside MOF-based MMMs.

Using the values of D_0 from Table 3, the normalized intra-ZIF self-diffusivities $D(t)/D_0$ were plotted as a function of $(D_0t)^{0.5}$ in Fig. S9 for all studied samples. Least square fittings of the data in Fig. S9 to Eq. (4) allowed obtaining the values of $f/3R$, which are shown in Table 3. Significant deviations of the experimental dependencies in Fig. S9 from the linear dependencies prescribed by Eq. (4) are not unexpected in view of a very broad distribution over the ZIF-71 crystal sizes (Fig. 5 and S1). The data in Table 3 show that for the same sorbate the values of $f/3R$ tend to be smaller in ZIF-71 crystal beds than in ZIF-71/Matrimid MMM and ZIF-71/Torlon MMM, respectively, by a factor of around 1.5 and 1.2. Assuming that the value of f remains the same for a particular sorbate type, these factors are in a satisfactory agreement with the decrease in the average crystal size by about a factor of 1.9 and 1.2, respectively, in ZIF-71/Matrimid MMM and ZIF-71/Torlon MMM in comparison to ZIF-71 crystal beds observed by SEM (Fig. 5 and S1). The data in Table 3 also allows estimating the values of f assuming R = 2.05, 1.7, and 1.1 μm for ZIF-71 crystal bed, ZIF-71/Torlon MMM, and ZIF-71/Matrimid MMM, respectively. The values of R were calculated by dividing by a factor of 2 the particle diameters (or sizes) obtained by SEM and discussed above. These values are shown in Table 3. It is seen that the value of f is, on average, larger for *o*-xylene than for *p*-xylene by a factor of around 1.9. This observation indicates that for larger *o*-xylene

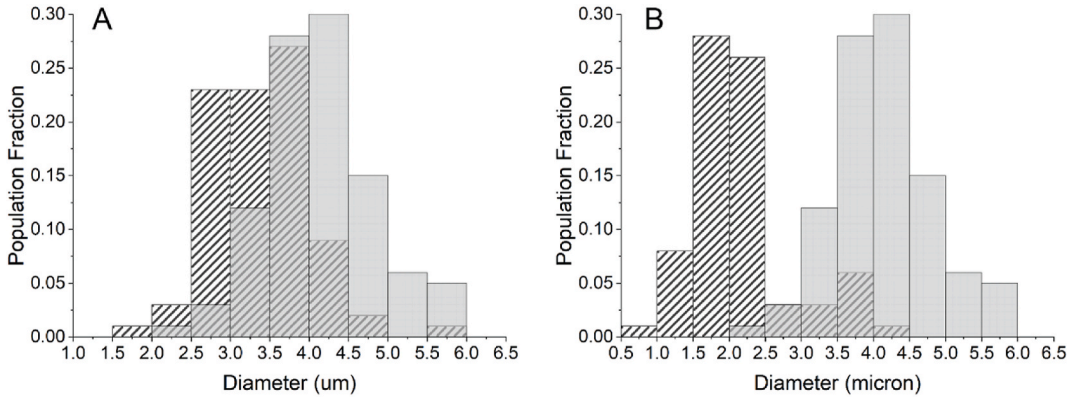

Fig. 5. Crystal size distribution histogram of ZIF-71-based MMMs prepared with crosslinked Torlon (A) and Matrimid (B) polymers obtained from SEM images (Fig. S4). The particle size distributions of the MMMs are shown as patterned columns. The particle size distribution of the neat ZIF crystals is overlaid as transparent gray. The average ZIF-71 crystal sizes in the crosslinked membranes were estimated to be around 3.4 μm for ZIF-71/Torlon MMM (A) and around 2.2 μm for ZIF-71/Matrimid MMM (B).

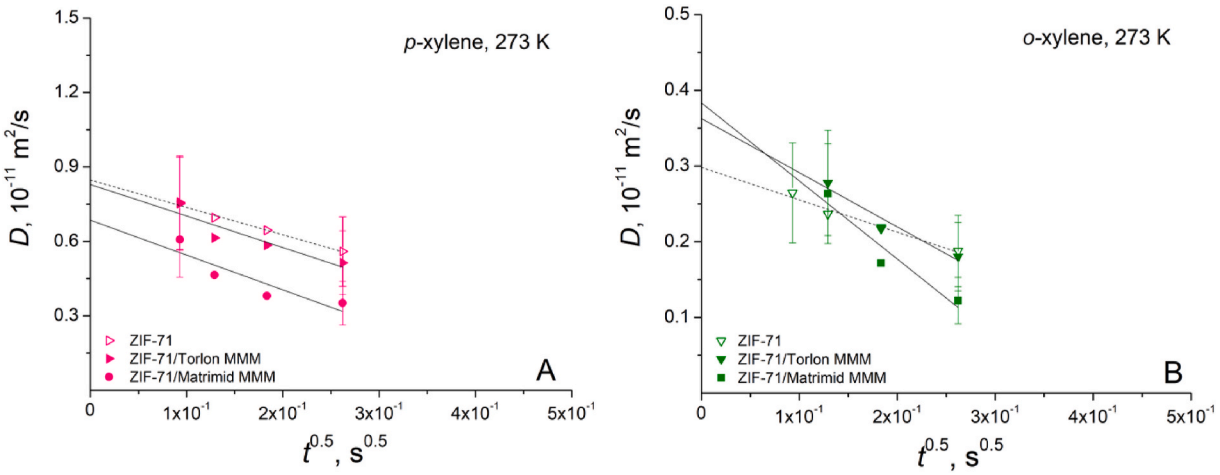

Fig. 6. *P*-xylene (A) and *o*-xylene (B) self-diffusivities as a function of $t^{0.5}$ for studied ZIF-71 crystal beds (hollow symbols) and ZIF-71 based MMMs (filled symbols) samples at 273 K and 14 T. The solid and dotted lines represent the best fit lines obtained by fitting the data using Eq. (4).

Table 3
Values of intracrystalline diffusivities in the limit of small diffusion times (D_0) and $f/3R$ obtained by fitting the PFG NMR data using Eq. (4). The values of f were calculated from the values of $f/3R$ assuming R = 2.05, 1.7, and 1.1 μm for ZIF-71 crystal bed, ZIF-71/Torlon MMM, and ZIF-71/Matrimid MMM, respectively.

Sample	D_0 (10^{-10} m^2/s)	$f/3R$ (10^5 m^{-1})	F
ZIF-71 loaded with *p*-xylene	0.085 ± 0.021	8.1	5
ZIF-71 loaded with *o*-xylene	0.030 ± 0.008	14.8	9
ZIF-71/Torlon MMM loaded with *p*-xylene	0.083 ± 0.021	9.3	5
ZIF-71/Torlon MMM loaded with *o*-xylene	0.036 ± 0.009	18.2	9
ZIF-71/Matrimid MMM loaded with *p*-xylene	0.069 ± 0.017	13.4	4
ZIF-71/Matrimid MMM loaded with *o*-xylene	0.038 ± 0.010	23.9	8

molecules the ZIF-71 external crystal surface has a more reflective character than for smaller *p*-xylene molecules. A good agreement observed for any particular sorbate between the values of f for the ZIF-71 crystal bed and those for the MMMs suggest that the crystal surface permeance for the studied sorbates was not significantly influenced by the crystal confinement in the polymers and the polymer crosslinking process. Clearly, the deviations of the values for f in Table 3 from the value of $f = 4$ and 2, respectively, for reflecting and adsorbing external surface of a sphere can be attributed to the existence of a broad distribution over ZIF-71 crystal sizes and shapes in the studied samples with smaller crystals contributing significantly to the PFG NMR data. The results in Table 3 indicates that the intra-ZIF diffusion selectivity, which can be defined as a ratio of the D_0 values for *p*-xylene and *o*-xylene, is maintained at the applications-attractive level of about 3 in both studied MMMs despite the crystal degradation.

The values of D_0 represent the intra-membrane diffusivities in the limit when the intra-ZIF diffusion process starts dominating the overall diffusion in the MMMs, i.e., for large ZIF volume fractions and no significant diffusion restrictions at the ZIF/polymer interfaces in the MMMs. Direct access to these values from PFG NMR measurements will allow for a better understanding of the relationship between the macroscopic diffusion rates, which can be readily measured in permeation experiments for the entire membrane, and the corresponding microscopic diffusion inside the filler particles. Such understanding should facilitate knowledge-based optimization of the MMM formation.

4. Conclusion

^{13}C PFG NMR at 14 T and 273 K was applied to investigate self-diffusion of xylene isomers inside ZIF-71-based MMMs, which were modified by a polymer crosslinking process. The corresponding self-diffusion measurements were also performed for the reference samples of ZIF-71 crystal beds. It was observed that for any sorbate type, the intra-ZIF self-diffusivities obtained for all studied samples decrease as the diffusion time and corresponding root MSD values increase. These dependencies were attributed to the influence of the external crystal surface on the diffusion process. Quantitative analysis of these dependencies indicates that for each sorbate type the intra-ZIF diffusivity D_0, which is not influenced by any effects at the external crystal surface, remains the same for all studied samples. The reported D_0, values are also in agreement with the corresponding D_0 values previously obtained for the corresponding MMMs without any polymer modification. Hence, the polymer crosslinking process used have not influenced the intra-ZIF diffusion away from the crystal boundaries. In contrast, the quantitative analysis of the diffusion time dependent intra-ZIF diffusivities indicates that the crosslinking process resulted in a decrease of the ZIF-71 crystal sizes inside the MMMs. This effect was significantly more pronounced for ZIF-71/Matrimid MMMs. The observed crystal size decrease is attributed to a partial degradation of the ZIF-71 crystals inside the MMMs due to the crosslinking process. The latter conclusion was found to be in agreement with the results of SEM measurements. The reported PFG NMR data also suggests that for larger *o*-xylene molecules the ZIF-71 external crystal surface has a more reflective character than for smaller *p*-xylene molecules.

CRediT authorship contribution statement

Amineh Baniani: Writing – review & editing, Writing – original draft, Investigation, Formal analysis, Data curation. **Matthew P. Rivera:** Writing – review & editing, Investigation, Formal analysis, Data curation. **João Marreiros:** Data curation, Investigation. **Ryan P. Lively:** Writing – review & editing, Supervision, Funding acquisition, Formal analysis. **Sergey Vasenkov:** Writing – review & editing, Writing – original draft, Supervision, Project administration, Methodology, Investigation, Funding acquisition.

Declaration of competing interest

All authors of this manuscript certify that they have NO affiliations with or involvement in any organization or entity with any financial interest (such as honoraria; educational grants; participation in

speakers' bureaus; membership, employment, consultancies, stock ownership, or other equity interest; and expert testimony or patent-licensing arrangements), or non-financial interest (such as personal or professional relationships, affiliations, knowledge or beliefs) in the subject matter or materials discussed in this manuscript.

Data availability

Data will be made available on request.

Acknowledgments

The present work was financially supported by NSF (CBET awards No. 1836735 and No. 1836738). A portion of this work was performed in the McKnight Brain Institute at the National High Magnetic Field Laboratory's AMRIS Facility, which is supported by National Science Foundation Cooperative Agreement No. DMR-1157490 and the State of Florida. This work was supported in part by an NIH award, S10RR031637, for magnetic resonance instrumentation.

Appendix A. Supplementary data

Supplementary data to this article can be found online at https://doi.org/10.1016/j.micromeso.2023.112648.

References

[1] C. Zhang, Y. Dai, J.R. Johnson, O. Karvan, W.J. Koros, High performance ZIF-8/6FDA-DAM mixed matrix membrane for propylene/propane separations, J. Membr. Sci. 389 (2012) 34–42.
[2] D. Qadir, H. Mukhtar, L.K. Keong, Synthesis and characterization of polyethersulfone/carbon molecular Sieve based mixed matrix membranes for water treatment application, Procedia Eng. 148 (2016) 588–593.
[3] M. Maghami, A. Abdelrasoul, Zeolite Mixed Matrix Membranes (Zeolite-MMMs) for Sustainable Engineering, Zeolites and Their Applications, 2018.
[4] M.Z. Ahmad, V. Martin-Gil, T. Supinkova, P. Lambert, R. Castro-Muñoz, P. Hrabanek, M. Kocirik, V. Fila, Novel MMM using CO_2 selective SSZ-16 and high-performance 6FDA-polyimide for CO_2/CH_4 separation, Sep. Purif. Technol. 254 (2021), 117582.
[5] M.W. Anjum, B. Bueken, D.D. Vos, I.F.J. Vankelecom, MIL-125(Ti) based mixed matrix membranes for CO_2 separation from CH_4 and N_2, J. Membr. Sci. 502 (2016) 21–28.
[6] N. Tien-Binh, D. Rodrigue, S. Kaliaguine, In-situ cross interface linking of PIM-1 polymer and UiO-66-NH2 for outstanding gas separation and physical aging control, J. Membr. Sci. 548 (2018) 429–438.
[7] G. Yilmaz, S. Keskin, Predicting the performance of zeolite imidazolate framework/polymer mixed matrix membranes for CO_2, CH_4, and H_2 separations using molecular simulations, Ind. Eng. Chem. Res. 51 (2012) 14218–14228.
[8] T. Li, Y. Pan, K.-V. Peinemann, Z. Lai, Carbon dioxide selective mixed matrix composite membrane containing ZIF-7 nano-fillers, J. Membr. Sci. 425–426 (2013) 235–242.
[9] A.F. Ismail, W.R. Rahman, F. Aziz, Development of polysulfone (PSF)-Carbon molecular Sieve (CMS) mixed matrix membrane (MMM) for O_2/N_2 gas separation, AIP Conf. Proc. 1136 (2009) 201–206.
[10] C.I. Chaidou, G. Pantoleontos, D.E. Koutsonikolas, S.P. Kaldis, G. P. Sakellaropoulos, Gas separation properties of polyimide-zeolite mixed matrix membranes, Separ. Sci. Technol. 47 (2012) 950–962.
[11] S. Saqib, S. Rafiq, N. Muhammad, A.L. Khan, A. Mukhtar, S. Ullah, M.H. Nawaz, F. Jamil, C. Zhang, V. Ashokkumar, Sustainable mixed matrix membranes containing porphyrin and polysulfone polymer for acid gas separations, J. Hazard Mater. 411 (2021).
[12] R.C. Dutta, S.K. Bhatia, Interfacial engineering of MOF-based mixed matrix membrane through atomistic simulations, J. Phys. Chem. C 124 (2020) 594–604.
[13] K.S. Park, Z. Ni, A.P. Côté, J.Y. Choi, R. Huang, F.J. Uribe-Romo, H.K. Chae, M. O'Keeffe, O.M. Yaghi, Exceptional chemical and thermal stability of zeolitic imidazolate frameworks, PNAS 103 (2006) 10186–10191.
[14] P.A. Banerjee R, B. Wang, C. Knobler, H. Furukawa, M. O'Keeffe, O.M. Yaghi, High-throughput synthesis of zeolitic imidazolate frameworks and application to CO2 capture, Science 319 (2008) 939–943.
[15] B.R. Pimentel, A. Parulkar, E.-k. Zhou, N.A. Brunelli, R.P. Lively, Zeolitic imidazolate frameworks: next-generation materials for energy-efficient gas separations, Chem. Sustain. Energy Mater. 7 (2014) 3202–3240.
[16] A. Baniani, C. Chmelik, E.M. Forman, L. Fan, K.J. Ziegler, E. Zhou, F. Zhang, R. Lyndon, R.P. Lively, S. Vasenkov, Anomalous relationship between molecular size and diffusivity of ethane and ethylene inside crystals of zeolitic imidazolate framework-11, J. Phys. Chem. C 123 (2019) 16813–16822.
[17] X. Zhang, T. Zhang, Y. Wang, J. Li, C. Liu, N. Li, J. Liao, Mixed-matrix membranes based on Zn/Ni-ZIF-8-PEBA for high performance CO_2 separation, J. Membr. Sci. 560 (2018) 38–46.
[18] S. Meshkat, S. Kaliaguine, D. Rodrigue, Comparison between ZIF-67 and ZIF-8 in Pebax® MH-1657 mixed matrix membranes for CO_2 separation, Sep. Purif. Technol. 235 (2020), 116150.
[19] W. Wei, J. Liu, J. Jiang, Atomistic simulation study of polyarylate/zeolitic-imidazolate framework mixed-matrix membranes for water desalination, ACS Appl. Nano Mater. 3 (2020) 10022–10031.
[20] A.B. Yumru, M.S. Boroglu, I. Boz, ZIF-11/Matrimid® mixed matrix membranes for efficient CO_2,CH_4,and H_2 separations, Greenh. Gases: Sci. Technol. 8 (2018) 529–541.
[21] A.W. Thornton, D. Dubbeldam, M.S. Liu, B.P. Ladewig, A.J. Hill, M.R. Hill, Feasibility of zeolitic imidazolate framework membranes for clean energy applications, Energy Environ. Sci. 5 (2012) 7637–7646.
[22] J. Sánchez-Laínez, B. Zornoza, C. Téllez, J. Coronas, On the chemical filler–polymer interaction of nano- and micro-sized ZIF-11 in PBI mixed matrix membranes and their application for H_2/CO_2 separation, J. Mater. Chem. A 4 (2016) 14334–14341.
[23] A. Guo, Y. Ban, K. Yang, Y. Zhou, N. Cao, M. Zhao, Weishen Yang, Molecular sieving mixed matrix membranes embodying nano-fillers with extremely narrow pore-openings, J. Membr. Sci. 601 (2020), 117880.
[24] A. Ozcan, R. Semino, G. Maurin, A.O. Yazaydin, Modeling of gas transport through polymer/MOF interfaces: a microsecond-scale concentration gradient-driven molecular dynamics study, Chem. Mater. 32 (2020) 1288–1296.
[25] M.S. Boroglu, A.B. Yumru, Gas separation performance of 6FDA-DAM-ZIF-11 mixed-matrix membranes for H_2/CH_4 and CO_2/CH_4 separation, Sep. Purif. Technol. 173 (2017) 269–279.
[26] W. Li, S.A.S.C. Samarasinghe, Tae-Hyun Bae, Enhancing CO_2/CH_4 separation performance and mechanical strength of mixed-matrix membrane via combined use of graphene oxide and ZIF-8, J. Ind. Eng. Chem. 67 (2018) 156–163.
[27] S. Liu, G. Liu, X. Zhao, W. Jin, Hydrophobic-ZIF-71 filled PEBA mixed matrix membranes for recovery of biobutanol via pervaporation, J. Membr. Sci. 446 (2013) 181–188.
[28] Y. Li, L.H. Wee, J.A. Martens, I.F.J. Vankelecom, ZIF-71 as a potential filler to prepare pervaporation membranes for bio-alcohol recovery, J. Mater. Chem. A 2 (2014) 10034–10040.
[29] H. Yin, C.Y. Lau, M. Rozowski, C. Howard, Y. Xu, T. Lai, M.E. Dose, R.P. Lively, M. L. Lind, Free-standing ZIF-71/PDMS nanocomposite membranes for the recovery of ethanol and 1-butanol from water through pervaporation, J. Membr. Sci. 529 (2017) 286–292.
[30] W. Morris, B. Leung, H. Furukawa, O.K. Yaghi, N. He, H. Hayashi, Y. Houndonougbo, M. Asta, B.B. Laird, O.M. Yaghi, A combined Experimental–Computational investigation of carbon dioxide capture in a series of isoreticular zeolitic imidazolate frameworks, J. Am. Chem. Soc. 132 (2010) 11006–11008.
[31] E.M. Forman, A. Baniani, L. Fan, K.J. Ziegler, E. Zhou, F. Zhang, R.P. Lively, S. Vasenkov, Relationship between ethane and ethylene diffusion inside ZIF-11 crystals confined in polymers to form mixed-matrix membranes, J. Membr. Sci. 593 (2020).
[32] A. Baniani, S.J. Berens, M.P. Rivera, R.P. Lively, S. Vasenkov, Potentials and Challenges of High-Field PFG NMR Diffusion Studies with Sorbates in Nanoporous Media, Adsorption, 2021.
[33] E.M. Forman, A. Baniani, L. Fan, K.J. Ziegler, E. Zhou, F. Zhang, R.P. Lively, S. Vasenkov, Ethylene diffusion in crystals of zeolitic imidazole framework-11 embedded in polymers to form mixed-matrix membranes, Microporous Mesoporous Mater. 274 (2019) 163–170.
[34] L. Diestel, N. Wang, B. Schwiedland, F. Steinbach, U. Giese, J. Caro, MOF based MMMs with enhanced selectivity due to hindered linker distortion, J. Membr. Sci. 492 (2015) 181–186.
[35] R. Mueller, S. Zhang, C. Zhang, R.P. Lively, S. Vasenkov, Relationship between long-range diffusion and diffusion in the ZIF-8 and polymer phases of mixed-matrix membrane by high field NMR diffusometry, J. Membr. Sci. 477 (2015) 123–130.
[36] R. Mueller, V. Hariharan, C. Zhang, R. Lively, S. Vasenkov, Relationship between mixed and pure gas self-diffusion for ethane and ethene in ZIF-8/6FDA-DAM mixed-matrix membrane by pulsed field gradient NMR, J. Membr. Sci. 499 (2016) 12–19.
[37] S. Friebe, A. Mundstock, K. Volgmann, J. Caro, On the better understanding of the surprisingly high performance of Metal–Organic framework-based mixed-matrix membranes using the example of UiO-66 and Matrimid, ACS Appl. Mater. Interfaces 9 (2017) 41553–41558.
[38] A. Baniani, M.P. Rivera, R.P. Lively, S. Vasenkov, Quantifying diffusion of organic liquids in a MOF component of MOF/polymer mixed-matrix membranes by high field NMR, J. Membr. Sci. 640 (2021), 119786.
[39] A. Baniani, M.P. Rivera, R.P. Lively, S. Vasenkov, Self-diffusion of mixed xylene isomers in ZIF-71 crystals dispersed in a polymer to form a hybrid membrane, Microporous Mesoporous Mater. 338 (2022), 111960.
[40] R.M. Cotts, M.J.R. Hoch, T. Sun, J.T. Markert, Pulsed field gradient stimulated echo methods for improved NMR diffusion measurements in heterogeneous systems, J. Magn. Reson. 83 (1989) 252–266.
[41] S.J. Gibbs, C.S. Johnson, A PFG NMR experiment for accurate diffusion and flow studies in the presence of eddy currents, J. Magn. Reson. 93 (1991) 395–402.
[42] J. Kärger, D.M. Ruthven, D.N. Theodorou, Diffusion in Nanoporous Materials, Wiley-VCH Verlag GmbH & Co. KGaA, Weinheim, Germany, 2012.
[43] J. Kärger, H. Pfeifer, W. Heink, Principles and application of self-diffusion measurements by NMR, Adv. Magn. Reson. 12 (1988) 1–89.

[44] J. Kärger, M. Avramovska, D. Freude, J. Haase, S. Hwang, R. Valiullin, Pulsed Field Gradient NMR Diffusion Measurement in Nanoporous Materials, Adsorption, 2020.
[45] P.T. Callaghan, D. MacGowan, K.J. Packer, F.O. Zelaya, Influence of field gradient strength in NMR studies of diffusion in porous media, Magn. Reson. Imaging 9 (1991) 663–671.
[46] E.O. Stejskal, J.E. Tanner, Spin diffusion measurements: spin echoes in the presence of a time-dependent field gradient, J. Chem. Phys. 42 (1965) 288–292.
[47] P. Galvosas, F. Stallmach, G. Seiffert, J. Kärger, U. Kaess, G. Majer, Generation and application of ultra-high-intensity magnetic field gradient pulses for NMR spectroscopy, J. Magn. Reson. 151 (2001) 260–268.
[48] S. Bhattacharyya, R. Han, W.-G. Kim, Y. Chiang, K.C. Jayachandrababu, J. T. Hungerford, M.R. Dutzer, C. Ma, K.S. Walton, D.S. Sholl, S. Nair, Acid gas stability of zeolitic imidazolate frameworks: generalized kinetic and thermodynamic characteristics, Chem. Mater. 30 (2018) 4089–4101.
[49] W.A.A. Arafa, H.M. Ibrahim, A sustainable strategy for the synthesis of bis-2-iminothiazolidin-4-ones utilizing novel series of asymmetrically substituted bis-thioureas as viable precursors, RSC Adv. 8 (2018) 10516–10521.
[50] P.P. Mitra, P.N. Sen, Effects of microgeometry and surface relaxation on NMR pulsed-field-gradient experiments: simple pore geometries, Phys. Rev. B: Condens. Matter 45 (1992) 143–156.
[51] P.P. Mitra, P.N. Sen, L.M. Schwartz, Short-time behavior of the diffusion coefficient as a geometrical probe of porous media, Phys. Rev. B: Condens. Matter 47 (1993) 8565–8574.